

Ideal Quantum non-demolishing measurement of a flux qubit at variable bias

Ying-Dan Wang,¹ Xiaobo Zhu,² and Christoph Bruder¹

¹*Department of Physics, University of Basel, Klingelbergstrasse 82, 4056 Basel, Switzerland*

²*NTT Basic Research Laboratories, NTT Corporation, 3-1, Morinosato Wakamiya, Atsugi-shi, Kanagawa 243-0198, Japan*

We propose a scheme to realize a quantum non-demolition (QND) measurement of a superconducting flux qubit by a Josephson bifurcation amplifier. Our scheme can implement a perfect QND measurement for a qubit subject to a variable magnetic bias. Measurement back-action induced qubit relaxation can be suppressed and hence the QND fidelity is expected to be high over a wide range of bias conditions.

PACS numbers: 03.67.Bg, 85.25.Cp, 03.67.Lx

I. INTRODUCTION

Quantum non-demolition (QND) measurements enable repeated measurements on quantum objects with accuracy levels exceeding the standard quantum limit¹. Such QND measurements on superconducting flux qubits have been reported^{2,3}. However, these QND schemes work only far away from the degeneracy point (the ‘sweet spot’ where the sensitivity to noise is minimized), and the QND criterion is only approximately satisfied. Here we propose an ideal QND measurement scheme of a flux qubit that can be applied in a wide range of bias conditions. The QND fidelity for this measurement is expected to increase significantly as compared to previous proposals.

In quantum mechanics, measurements induce back-action to the system under investigation due to Heisenberg uncertainty. This back-action puts a fundamental limit on the precision of repeated measurements. In order to beat the standard quantum limit^{1,4}, the concept of QND measurement was developed in the context of gravitational wave detection where repeated measurements beyond the standard quantum limit are required⁵. This concept has been extended from gravitational wave detection to other physical systems. A number of experiments has been performed in a micromechanical system⁶ and quantum optical systems⁷. This special type of measurement leaves the output state unaffected by subsequent measurements and the free evolution of the system. QND measurements are crucial to overcome detector inefficiencies, and to quantify the external disturbance to the QND variables. It is also found to have more versatile applications such as error correction⁸, one-way quantum computing⁹, low-noise amplification¹⁰ and entanglement generation^{11,12}.

In superconducting qubit systems, weak continuous QND measurements on superconducting transmon qubits have been realized in the dispersive limit¹³. This circuit QED system has also been used to detect single microwave photons in a coplanar wave guide¹⁴. Using the Josephson bifurcation amplifier, strong projective QND measurements have been demonstrated for quantum qubits, flux qubits, and transmon qubits^{2,15,16}. In order to implement QND detection for a continuous QND vari-

able, a number of criteria have to be satisfied^{4,5}. Among them, the most restrictive one is that the system free Hamiltonian H_s commutes with the interaction H_{int} between the system and the detector, i.e., $[H_s, H_{int}] = 0$. For existing flux qubit measurements^{2,3}, this QND criterion is only approximately satisfied when the qubit is biased far away from the degeneracy point. However, the quantum coherence times for solid-state qubit vanish rapidly in this regime. QND detection close to the qubit degeneracy point is therefore desired. Moreover, to acquire full qubit control, the qubit bias has to be changed during various operations. After implementing an operation at a certain bias, it is desirable to be able to carry out a QND measurement at that point, without adiabatically shifting back to another bias value. In this paper, by introducing an rf SQUID coupler to mediate the interaction between a flux qubit and the detector, a Josephson bifurcation amplifier (JBA), we find a detection scheme that allows to implement a QND measurement at arbitrary bias including the degeneracy point. Moreover, our scheme works beyond the dispersive limit and can be extended to the case of strong qubit-detector coupling. This will help to improve the readout contrast to achieve a higher measurement fidelity and shorter measurement times.

Another advantage of this scheme is the possibility to improve the so-called QND fidelity, which quantifies the accuracy of repeated measurements. In QND measurements by a JBA^{2,15}, the drive on the JBA is first ramped to the bifurcation point to induce transitions between two bistable states. It is then reduced to maintain a latching plateau. The circuit geometry in the previous experiments does not implement an ideal QND measurement, i.e., $[H_s, H_{int}] \neq 0$. Qubit relaxation is then accelerated by the forced oscillations of the nonlinear resonator. The population fraction lost during the latching plateau and the preparation stage of the subsequent measurement limit the accuracy of the subsequent measurement. It turns out that the JBA induced qubit relaxation is the main limiting factor for the QND fidelity¹⁷. In our design, if proper control on the bias is acquired, the detection scheme is an ideal QND measurement. The QND fidelity is only limited by environment-induced qubit re-

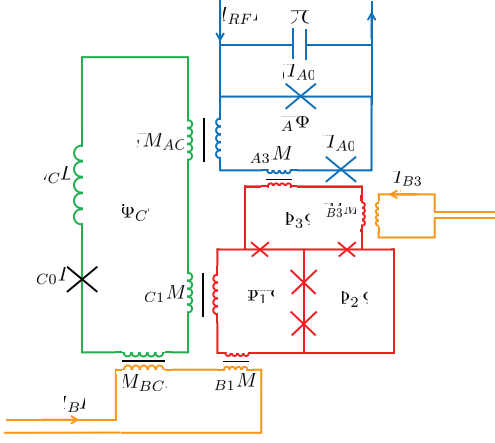


FIG. 1: (Color online) Schematic diagram of the circuit. Red part: gradiometer flux qubit to be measured. Blue part: measurement device, a Josephson bifurcation amplifier formed by a dc SQUID shunted by a capacitance. Green part: rf SQUID acting as a tunable coupler. Orange parts: bias circuits.

laxation, which is usually one order of magnitude smaller than the JBA induced relaxation.

The structure of this paper is as follows: In Sec. II, we describe the circuit layout and the effective mutual inductance between the qubit and the JBA. The QND feature of this detection is analyzed in Sec. III, where two situations with bias at and off the degeneracy point are discussed respectively. In Sec. IV, we revisit the working principle of the JBA and calculate the qubit relaxation rates in the measurement process. With those relaxation rates, the fidelity of the QND measurement is evaluated. Section V discusses and summarizes our results.

II. THE CIRCUIT LAYOUT

Previous measurements can only work in the regime far away from the degeneracy point. This is because the measurement circuit (e.g. a Josephson bifurcation amplifier) can only be coupled to supercurrents in the loop. However in the conventional 3-Josephson junction design^{18,19}, the current states are the eigenstates of the system only if the qubit is biased to the degeneracy point. A natural solution for this problem is to use a gap-tunable qubit^{20–22} and couple the measurement device to the dc SQUID part. This will enable a QND measurement when the qubit is biased at the degeneracy point. However, to implement a QND measurement at variable bias, the coupling with the measurement device has to be mediated in a way that it can always follow the eigenstates of the system. In this paper, we introduce a tunable coupler between the flux qubit and the Josephson bifurcation amplifier. The qubit shares one control line with the tunable coupler. As the qubit bias is varied, the qubit coupling to the Josephson bifurcation amplifier is modified simulta-

neously. We find that under certain conditions, a perfect QND measurement can be performed at variable qubit bias.

The system we have in mind is shown in Fig. 1. It is composed of four parts: the system to be measured (red part), the measuring apparatus (blue part), the coupler (green part) and the bias circuits (orange parts). The system to be measured is a gradiometer-type superconducting flux qubit^{20,21} which contains four Josephson junctions in three loops: The two lower loops (the main qubit loops) and the upper loop (the dc SQUID loop) penetrated by magnetic fluxes Φ_1 , Φ_2 , and Φ_3 . The two junctions in the dc SQUID loop are assumed to have identical Josephson energies $\alpha_0 E_J$, here α_0 is the ratio between the Josephson energy of the smaller junctions and that of the two bigger junctions. The other two junctions are assumed to have the Josephson energy E_J . The total Josephson energy of the circuit is²³

$$E_J \cos \varphi_1 + E_J \cos \varphi_2 + \alpha E_J \cos (2\pi \Phi_t / \Phi_0 - (\varphi_1 + \varphi_2)) \quad (1)$$

where $\Phi_t \equiv (\Phi_1 - \Phi_2)/2$, $\alpha = 2\alpha_0 \cos(\pi \Phi_3 / \Phi_0)$, and φ_k ($k = 1, 2, 3, 4$) is the phase difference across the k -th Josephson junction. If Φ_t is chosen close to $\Phi_0/2$ where $\Phi_0 = h/(2e)$ is the flux quantum, the circuit dynamics can be effectively described in a two-level subspace of a double-well potential, and thus constitutes a flux qubit^{18,19}. Together with the charging energy, the total Hamiltonian of the qubit is

$$H = \varepsilon(\Phi_t) \sigma_z + \Delta(\Phi_3) \sigma_x. \quad (2)$$

The Pauli matrices read $\sigma_z = |0\rangle\langle 0| - |1\rangle\langle 1|$, $\sigma_x = |0\rangle\langle 1| + |1\rangle\langle 0|$, where $|0\rangle$ and $|1\rangle$ denote the states with clockwise and counterclockwise currents in the outer loop. The energy spacing of the two current states is $\varepsilon(\Phi_t) \equiv I_p(\Phi_t - \Phi_0/2)$, with I_p the magnitude of the classical persistent current in the loop. The tunneling amplitude between the two states $\Delta(\Phi_3) \equiv \Delta(\alpha)$ depends on the bias in the dc SQUID loop. Note that in contrast to the original flux qubit design^{18,19}, this gradiometer flux qubit is insensitive to homogeneous fluctuations of the magnetic flux²⁰. More importantly, it enables the JBA to couple with the dc-SQUID loop without changing the total bias flux of the qubit.

The detector for the flux qubit is a Josephson bifurcation amplifier (JBA)²⁴ (blue part in Fig. 1), which in our scheme is a dc SQUID shunted by a capacitance C , subject to a microwave drive $I_{RF} \cos(\omega_d t + \phi_A)$. The JBA SQUID loop contains two identical Josephson junctions of critical current I_{A0} . The phase differences across the two junctions are denoted by φ_{A1} , φ_{A2} respectively. The current in the loop is $I_A = \bar{I}_A(\Phi_A) \cos \varphi_A$, with Φ_A , the flux bias in the JBA SQUID, set by external coils, $\bar{I}_A(\Phi_A) = 2I_{A0} \sin(\pi \Phi_A / \Phi_0)$, and $\varphi_A = (\varphi_{A1} + \varphi_{A2})/2$. The JBA circuit forms a driven nonlinear resonator which exhibits bistable behavior with hysteresis. With appropriate drive sequences, a transition to one of the bistable states is correlated with the qubit states in a probabilis-

tic way. Therefore the qubit state can be read out by the phase of the transmitted or reflected microwave.

The flux qubit is coupled to the JBA through their mutual inductance. There are two contributions to their mutual inductance: the direct mutual inductance (DMI) M_{Ak} ($k = 1, 2$, and 3 denotes the different loops in the qubit) and the effective mutual inductance (EMI) M'_{Ak} . Hence the JBA produces flux biases to the qubit loops of the form $(M_{Ak} + M'_{Ak})I_A$. The EMI is induced by the nearby rf SQUID which acts as a coupler for the qubit and the JBA. The self-inductance of the coupler is assumed to be much larger than the mutual inductances and the dynamics of the coupler is confined to its lowest energy bands^{25,26}. The DMI is fixed by fabrication processes while the EMI is tunable by the magnetic bias of the coupler Φ_C as^{25,27}

$$M'_{Ak}(\Phi_C) = -\frac{M_{AC}M_{Ck}}{L_C} \frac{\beta_c \cos \theta_0}{1 + \beta_c \cos \theta_0}, \quad (3)$$

where θ_0 satisfies the nonlinear equation

$$\theta_0 = \frac{2\pi}{\Phi_0}(\Phi_C + M_{AC}I_{A0}) - \beta_c \sin \theta_0 \quad (4)$$

with $\beta_c = 2\pi L_C I_{C0}/\Phi_0$, L_C is the self-inductance of the coupler, and I_{C0} the circulating coupler current. In particular, if the coupler is biased at $\Phi_C = ((2n+1/2)\pi + \beta_c)\Phi_0/2\pi - M_{AC}I_{A0}$ or $((2n+3/2)\pi - \beta_c)\Phi_0/2\pi - M_{AC}I_{A0}$ (n is an arbitrary integer), the effective mutual inductance vanishes, $M'_{Ak} = 0$. Thus, for this bias condition, the EMIs between the JBA and all the qubit loops are canceled, and only the DMIs contribute to the coupling.

Besides tunability, there is another important difference between the DMI and the EMI: the DMI is symmetric with respect to the qubit loops 1 and 2, while the EMI is not symmetrical, that is, $M_{A1} = M_{A2}$, while $M'_{A1} \neq M'_{A2}$ (since $M_{C1} \neq M_{C2}$). Hence only the EMI couples the JBA to the gradiometer qubit flux Φ_t in the form

$$\Phi_t = (M'_{A1} - M'_{A2})I_A. \quad (5)$$

In our scheme, the whole chip is biased by external coils so that a homogeneous magnetic field threads all the loops. By choosing the area of each loop appropriately, the required background bias values can be imposed. Besides the coupling to the external coils, the dc SQUID loop of the qubit is also coupled with an on-chip bias current I_{B3} through M_{B3} . The qubit loop 1 shares another on-chip bias (the lower orange part) with the coupler. A bias current I_B in this bias line couples to the qubit loops and the coupler loop through mutual inductances M_{Bk} and M_{BC} . In the following discussion, we will see that this shared bias is crucial for the possibility to do a QND measurement at arbitrary bias.

III. QND NATURE OF THE DETECTION SCHEME

In order to analyze the QND nature of the detection scheme, we first look at the situation that the bias is set at the degeneracy point and then study the case of a general (off-degeneracy) bias.

A. Degeneracy point

We first look at the case when the qubit is biased at the degeneracy point $\Phi_{tb} = \Phi_0/2$. At this point, the first-order flux noise disappears so that the qubit quantum coherence can be preserved longer.

The qubit is biased at the degeneracy point by trapping one flux quantum^{20,21}. The bias current is set to zero $I_B = 0$ and the flux bias of the coupler is set by external coils to be

$$\Phi_{Cb} = \frac{\Phi_0}{2\pi} \left(\frac{\pi}{2} + \beta_c \right) - M_{AC}\bar{I}_A. \quad (6)$$

According to the discussion following Eq. (3), the effective mutual inductance M'_{Ak} vanishes at this bias. Thus, the qubit only couples to the JBA through the direct mutual inductance. As shown in Eq. (5), this means the JBA has no influence on Φ_t , but only couples to Φ_3 . If $\pi M_{A3}\bar{I}_A \ll \Phi_0$, the Hamiltonian can be expanded to first order as²³

$$H_q = H_{q0} + H_I, \quad (7)$$

where H_{q0} is the free Hamiltonian of the qubit

$$H_{q0} = \Delta(\Phi_{3b})\sigma_x, \quad (8)$$

and H_I is the interaction between the qubit and the JBA

$$H_I = \lambda(\Phi_{3b})\sigma_x \cos \varphi_A. \quad (9)$$

where Φ_{3b} is the total flux bias of the dc SQUID loop (generated by both external coils and I_{B3}). The coupling coefficient is

$$\lambda(\Phi_{3b}) = -\frac{\pi M_{A3}\bar{I}_A}{\Phi_0} \kappa(\Phi_{3b}) \quad (10)$$

with

$$\kappa(\Phi_{3b}) = 2\alpha_0 \sin \left(\pi \frac{\Phi_{3b}}{\Phi_0} \right) \left. \frac{d\Delta(\alpha)}{d\alpha} \right|_{\alpha=\bar{\alpha}}$$

and $\bar{\alpha} = 2\alpha_0 \cos(\pi\Phi_{3b}/\Phi_0)$. The coupling energy between the qubit and the JBA is tunable by Φ_{3b} .

Equations (7) – (9) show that the free Hamiltonian commutes with the interaction Hamiltonian. If one chooses σ_x as the measurement observable, a QND measurement can be implemented.

B. General (off-degeneracy) bias

If we change the current in the shared bias by a small amount $I_B = \delta I_B$, the qubit is biased away from the degeneracy point, and the corresponding bias change in the qubit loop is $\delta\Phi_t = (M_{B1} - M_{B2})\delta I_B$. Since the coupler shares the same bias, the magnetic flux penetrating the coupler bias is also shifted by a small amount $M_{BC}\delta I_B$ ($M_{BC}\delta I_B \ll \Phi_{Cb}$ is always satisfied in the relevant operation regime). This will induce a non-zero effective mutual inductance $M'_{Ak}(\Phi_{Cb} + M_{BC}\delta I_B) = -(2\pi/\Phi_0)^2 I_{c0} M_{AC} M_{Ck} M_{BC} \delta I_B$. As we discussed after Eq. (5), a non-zero EMI will couple the JBA to the qubit flux bias Φ_t as well as Φ_3 . The qubit Hamiltonian under this bias reads

$$H_q = H_{q0} + H_I \quad (11)$$

with

$$H_{q0} = \Omega_z \sigma_z + \Omega_x \sigma_x \quad (12)$$

and the interaction Hamiltonian

$$H_I = (\lambda_z \sigma_z + \lambda_x (\Phi_{3b}) \sigma_x) \cos \varphi_A \quad (13)$$

with $\Omega_z = I_p \delta\Phi_t$, $\Omega_x = \Delta(\Phi_{3b})$ and

$$\lambda_z = I_p (M'_{A1} - M'_{A2}) \bar{I}_A, \quad (14)$$

$$\lambda_x(\Phi_{3b}) = \lambda(\Phi_{3b}) \left(1 + \frac{M'_{A3}}{M_{A3}} \right). \quad (15)$$

If we define a parameter $\eta = \lambda_z \Omega_x / \lambda_x \Omega_z$, it is straightforward to see that the free qubit Hamiltonian commutes with the interaction Hamiltonian when $\eta = 1$. Therefore, a sufficient condition to implement a QND measurement at variable flux bias is

$$\eta(\Phi_{3b}) = 4\pi \frac{M_{BC} I_{c0}}{\Phi_0} \frac{M_{C1}}{M_{B1}} \frac{M_{AC}}{M_{A3}} \frac{\Delta(\Phi_{3b})}{\kappa(\Phi_{3b})} = 1 \quad (16)$$

where we have neglected M_{B2} , M_{C2} , and M_{C3} since they are much smaller than the other mutual inductances.

In other words, if $\eta = 1$, as the qubit is biased away from the degeneracy point, the interaction with the JBA is changed accordingly, so that the interaction Hamiltonian always commutes with the qubit free Hamiltonian. This condition is possible to be satisfied experimentally, e.g., if $\alpha_0 = 0.4$, and the bias Φ_{3b} satisfies $\bar{\alpha} = 0.7$. At this bias, $\Delta/(d\Delta/d\bar{\alpha}) \approx -0.11^{28}$. If $I_{C0} = 1 \mu\text{A}$, $M_{BC} = 23.5 \text{ pH}$, $M_{C1} = 25 \text{ pH}$, $M_{B1} = 5 \text{ pH}$, $M_{AC} = 25 \text{ pH}$, $M_{A3} = 5 \text{ pH}$, then $\eta = 1$. Note that η depends on the bias Φ_{3b} which is tunable *in situ*, i.e., by tuning I_{B3} . Thus, errors in the fabrication process can be compensated to satisfy Eq. (16), the condition for QND detection. Note that Φ_{3b} is determined by this condition since all the other parameters are fixed by fabrication. Therefore, this QND scheme works for variable bias values of

the main qubit loop, but it does not work for variable bias values of the dc SQUID loop in the general case. However, we would also like to point out that if the qubit is biased away from the degeneracy point, by changing ε , any arbitrary single-qubit operation can be implemented; in this sense, it is not necessary to tune Φ_{3b} . Also, if the qubit is biased at the degeneracy point, which is also the situation in which tuning Φ_{3b} is meaningful, the QND measurement can be implemented for variable Φ_{3b} .

For $\eta = 1$, the results obtained for the degeneracy point and general (off-degeneracy) bias can be written in a uniform way as

$$H_{q0} = \Omega \tilde{\sigma}_z \quad (17)$$

with $\Omega = \sqrt{\Omega_x^2 + \Omega_z^2}$, and $\tilde{\sigma}_z = (\Omega_z \sigma_z + \Omega_x \sigma_x)/\Omega$. The interaction Hamiltonian is

$$H_I = \lambda \tilde{\sigma}_z \cos \varphi_A \quad (18)$$

with $\lambda = \sqrt{\lambda_z^2 + \lambda_x^2}$. At the degeneracy point, $\Omega_z = \lambda_z = 0$, so that $\tilde{\sigma}_z = \sigma_x$.

IV. MEASUREMENT FIDELITY

The JBA is an oscillator with nonlinear Josephson inductance. Under a strong microwave drive, the Josephson energy of the junction $-E_{JA} \cos \varphi_A$ is expanded beyond the harmonic approximation and the classical dynamics can be described by a Duffing oscillator²⁹. For a certain range of drive conditions, the nonlinear oscillator exhibits bistable behavior with hysteresis^{24,29}. The two possible stable states correspond to different oscillation amplitudes and phases, which can be distinguished by transmitted or reflected microwave signals^{2,15,16}. Switching between the two stable states happens when the drive power reaches a certain threshold. The switching probability depends on the value of the nonlinear inductance, which in our case depends on the states of the qubit through the mutual inductance. This is because the effective Josephson energy of the junctions of the JBA is modified by the interaction Eq. (18) as $E_{JA}(\tilde{\sigma}_z) = \bar{I}_A \Phi_0 / 2\pi - \lambda \tilde{\sigma}_z$. Therefore, measuring the phase of the transmitted microwave signal, one can read out the state of the qubit.

The back-action from the measurement device destroys the phase coherence of the qubit states during the read-out process. Besides dephasing, the back-action could also induce relaxation to the qubit. This is the case for a qubit Hamiltonian $H_{q0} = \Omega \tilde{\sigma}_z + \tilde{\Delta} \tilde{\sigma}_x$ with a small non-ideal QND fraction $\tilde{\Delta}$, see e.g. the QND measurement of Ref. 2 where $\tilde{\Delta}/\Omega \approx 0.34$. The JBA is strongly coupled to a dissipative environment while weakly coupled to the qubit. Hence it serves as a bath for the qubit. According to Eq. (18), the influence of the JBA on the qubit can be described by its correlation function

$$G(\omega) = \int_0^\infty dt e^{i\omega t} \langle \cos \varphi_A(t) \cos \varphi_A(0) \rangle, \quad (19)$$

and the induced decay rate can be calculated through the Fermi golden rule. The Bloch Redfield rates induced by the operation of the JBA are

$$\begin{aligned}\Gamma_r &= \frac{\lambda^2 \tilde{\Delta}}{\sqrt{\Omega^2 + \tilde{\Delta}^2}} \Re(G(\sqrt{\Omega^2 + \tilde{\Delta}^2})) \\ \Gamma_\varphi &= \frac{\lambda^2 \Omega}{\sqrt{\Omega^2 + \tilde{\Delta}^2}} \Re(G(0)),\end{aligned}\quad (20)$$

where Γ_r is the induced relaxation rate and Γ_φ is the induced dephasing rate. When the JBA is ramped to the measurement level and the latching plateau, the correlation function is prominently increased due to quantum activation³⁰. Qubit decay is enhanced by the measurement operation^{17,31}. This results in qubit relaxation and the measurement is driven away from the QND regime. This induced relaxation has been found to be the main source of measurement error^{2,17}. One way to reduce this back-action is working in the dispersive limit¹⁶. In our case, an ideal QND measurement is possible, i.e. $\tilde{\Delta} = 0$, so that $\Gamma_r = 0$, i.e., the JBA does not induce extra relaxation but only dephasing to the qubit. Hence the QND condition can be preserved better in our scheme and the QND fidelity can be improved.

Besides the induced decay rates Eq. (20), there is another decay mechanism due to the flux fluctuations of the environment. This will perturb the fluxes in the qubit loops as $\delta\Phi_t = \mu_t X$ and $\delta\Phi_3 = \mu_3 X$, where X represents an environmental operator (such as a two-level fluctuator) and μ_t (μ_3) characterizes its coupling strength to the different qubit loops. Hence the qubit is coupled to the environment as $\Delta H = \xi_t X \sigma_z + \xi_3 X \sigma_x$, with $\xi_t = I_p \Phi_0 \mu_t$ and $\xi_3 = -\pi \mu_3 \kappa(\Phi_{3b})/\Phi_0$. In the interaction picture

$$\begin{aligned}\Delta H_I &= (\xi_3 \sin \chi + \xi_t \cos \chi) X(t) \sigma'_z \\ &+ (\xi_3 \cos \chi - \xi_t \sin \chi) X(t) (\sigma'_+ e^{i\Omega t} + \sigma'_- e^{-i\Omega t}),\end{aligned}\quad (21)$$

with $\cos \chi = \varepsilon/\Omega$ and $\sin \chi = \Delta/\Omega$.

According to the Fermi golden rule, the relaxation rate is $\Gamma_{\downarrow,\uparrow} = (\xi_3 \cos \chi - \xi_t \sin \chi)^2 S_X(\omega = \pm\Omega)$, where $S_X(\omega) = \int_{-\infty}^{\infty} d\tau \langle X(\tau) X(0) \rangle e^{i\omega\tau}$ is the flux noise spectrum. In a real experiment, the flux noise could have multiple sources, such as two-level fluctuators inside the barrier, high-frequency noise from the control lines²⁰, and others. Therefore the noise spectrum may exhibit a complicated frequency dependence and have a strong sample dependence. In our discussion, we assume an Ohmic noise spectrum (f -noise) for the environment bath plus a few peaks due to two-level fluctuators

$$S_X(\omega) = \omega R_0 \left(\coth \left(\frac{\omega}{2k_B T_0} \right) + 1 \right) + \sum_i S_i \delta(\omega - \omega_i),\quad (22)$$

where R_0 is the Ohmic impedance and T_0 is the environmental temperature. The QND fidelity of two successive measurements is

$$F_{\text{QND}}(\tau) = \frac{p(e|e) + p(g|g)}{2} = \frac{\exp(-\Gamma_{\downarrow}\tau) + \exp(-\Gamma_{\uparrow}\tau)}{2}\quad (23)$$

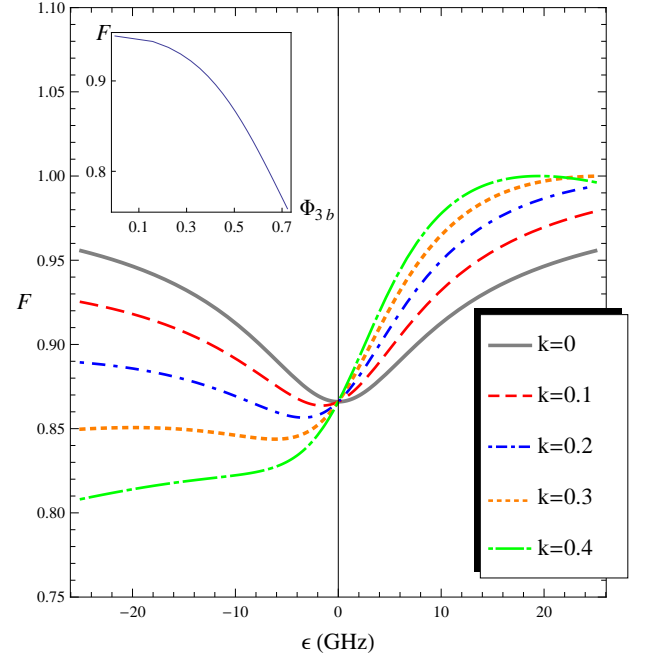


FIG. 2: (Color online) Dependence of the QND fidelity defined in Eq. (23) on the bias of the flux qubit for different values of $k = \xi_3/\xi_t$. Inset: dependence of the QND fidelity on the bias flux Φ_{3b} (in units of Φ_0/π) in the dc SQUID loop, when the qubit is biased at the degeneracy point.

where $p(e|e)$ ($p(g|g)$) is the probability that the qubit state $|e\rangle$ ($|g\rangle$) is unchanged after the first measurement and τ is the time interval between the two measurements.

Figure 2 shows the dependence of the QND fidelity on the qubit bias ε for different values of $k = \xi_3/\xi_t$ (usually $k < 1$ since the perturbation on the main qubit loop in general has a larger influence than the perturbation on the dc SQUID loop²⁸). Here we assume that the time interval between two measurements is $\tau = 50$ ns, $T_0 = 20$ mK, the qubit relaxation time is 250 ns at the degeneracy point, and the value of Δ is fixed at 7.8 GHz. The plot shows that the measurement fidelity remains rather high for a wide range of bias values. Even at the degeneracy point $\varepsilon = 0$ where the relaxation is strong, a measurement fidelity larger than 90% can be achieved. As the bias is increased to the positive side, the fidelity increases as the relaxation decreases. Far above the degeneracy point, the measurement fidelity is very close to 100%. Note that the fidelity is not symmetrical with respect to the axis $\varepsilon = 0$ but becomes more symmetrical as k decreases. At $k = 0$, the curve shows complete symmetry because noise only contributes to the main qubit loop, it is symmetrical with respect of the sign of the qubit bias. The inset of Fig. 2 shows that the QND fidelity at the degeneracy point decreases with the SQUID bias $\pi\Phi_{3b}/\Phi_0$. This is because at the degeneracy point, the qubit relaxation rate due to f -noise increases linearly with the gap Δ and Δ increases with the SQUID bias²⁸.

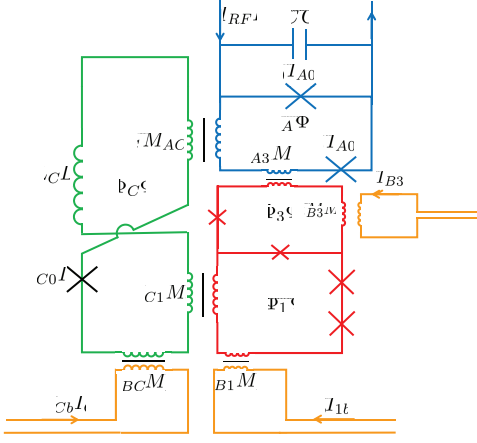


FIG. 3: (Color online) Schematic diagram of the circuit for a non-gradiometer qubit. Red part: non-gradiometer flux qubit to be measured. Blue part: measurement device, a Josephson bifurcation amplifier formed by a dc SQUID shunted by a capacitance. Green part: rf SQUID acting as a tunable coupler. Orange parts: bias circuits.

The measurement fidelity can be used as a noise spectrometer for environmental fluctuations. This is actually one of the main applications of QND measurements: detecting perturbations to the system. The QND nature of the measurement guarantees that the readout back-action will not change the value of the observable. The measurement fidelity therefore reflects the noise spectrum of the environment. For example, the existence of one two-level fluctuator inside the barrier^{32,33} would be revealed by a corresponding peak in the QND fidelity at a certain bias.

V. DISCUSSION AND SUMMARY

All the discussion above is based on the gradiometer type-flux qubit. However, with a few modifications as explained below, the measurement protocol can be adapted to non-gradiometer type flux qubits with a tunable gap²², see Fig. 3. Two current bias lines I_{Cb} and I_{lb} are used to control the coupler and the qubit separately in order to guarantee a QND measurement for a non-gradiometer flux qubit at the degeneracy point.

The background bias of a non-gradiometer qubit is sensitive to homogeneous magnetic field fluctuations, but can be implemented easily by external coils (while the gradiometer qubit requires the technique to trap fluxoids). Also, it is possible to achieve a more sensitive tuning comparing with the gradiometer qubit. This can be seen from Fig. 4 which shows the scaled effective mutual inductance with respect to the coupler bias. To achieve a more sensitive tuning within the tunable range of the on-chip bias (typically on the order of $m\Phi_0 \equiv 10^{-3}\Phi_0$), the coupler is desired to be pre-biased close to $\Phi_0/2$. How-

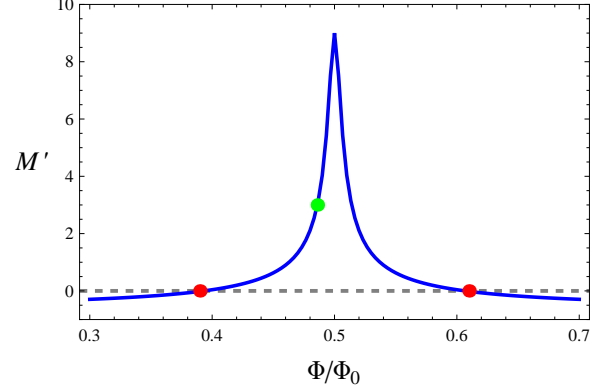


FIG. 4: (Color online) Dependence of the scaled effective mutual inductance $M' = M'_{Ak}/(M_{AC}M_{Ck}/L_C)$ on the coupler bias $\Phi = \Phi_{CB} + M_{AC}I_{A0}$, see Eq. (3). The red dots on the two sides (intersections with the dashed line) indicate the background bias in the case of the gradiometer qubit, while the green point in the middle is an example of the background bias for a non-gradiometer qubit. Here $\beta_c = 0.9$.

ever, in the case of the gradiometer qubit, since M'_{Ak} should be zero when the qubit is biased at the degeneracy point, the background bias should be set around the red points in Fig. 4, i.e., relatively far from $\Phi_0/2$. For non-gradiometer qubits, the background bias point is determined by the fabrication process. If the mutual inductance between the JBA and qubit is large and the coupler loop is twisted as indicated in Fig. 4, the background bias can be set closer to $\Phi_0/2$ (say, the green point in Fig. 4). As a result, a more sensitive tuning can be achieved. For example, if we assume $M_{A3} = 5$ pH, $M_{A1} = 0.5$ pH, $M_{AC} = 10$ pH, $L_C = 100$ pH, $M_{C1} = 10$ pH, $I_A = 1$ μ A, for a change in the qubit bias $\delta\Phi_t = 2$ $m\Phi_0$, the coupler bias Φ_{CB} should be tuned by 15 $m\Phi_0$ in the case of the gradiometer qubit, while only 0.4 $m\Phi_0$ in the case of a non-gradiometer qubit.

In summary, we have studied a scheme to realize a quantum non-demolition (QND) measurement for gradiometer-type flux qubits by a Josephson bifurcation amplifier. We have shown that a perfect QND measurement can be implemented for a qubit with variable magnetic bias. The QND fidelity of this measurement is expected to be high over a wide range of bias conditions. We have also discussed how to generalize our scheme to non-gradiometer qubits. Our estimates indicate that such a QND measurement may be realized experimentally, and we hope that this will happen in the close future.

VI. ACKNOWLEDGMENT

This work was financially supported by the EC IST-FET project SOLID, the Swiss SNF, and the NCCR

Nanoscience. Xiaobo Zhu was supported in part by the Funding Program for World-Leading Innovative R&D on Science and Technology (FIRST), and KAKENHI Nos. 18001002 and 22241025 by JSPS.

-
- ¹ V. B. Braginsky and F. Y. Khalili, *Rev. Mod. Phys.* **68**, 1 (1996).
 - ² A. Lupascu, S. Saito, T. Picot, P. C. D. Groot, C. J. P. M. Harmans, and J. E. Mooij, *Nature Physics* **3**, 119 (2007).
 - ³ T. Picot, R. Schouten, C. J. P. M. Harmans, and J. E. Mooij, *Phys. Rev. Lett.* **105**, 040506 (2010).
 - ⁴ V. B. Braginsky, Y. I. Vorontsov, and K. S. Thorne, *Science* **209**, 547 (1980).
 - ⁵ M. F. Bocko and R. Onofrio, *Rev. Mod. Phys.* **68**, 755 (1996).
 - ⁶ J. B. Hertzberg, T. Rocheleau, T. Ndukum, M. Savva, A. A. Clerk, and K. C. Schwab, *Nature Physics* **6**, 213 (2010).
 - ⁷ P. Grangier, J. A. Levenson, and J.-P. Poizat, *Nature* **396**, 537 (1998).
 - ⁸ A. M. Steane, *Phys. Rev. Lett.* **77**, 793 (1996).
 - ⁹ W. Dür and H.-J. Briegel, *Phys. Rev. Lett.* **90**, 067901 (2003).
 - ¹⁰ J. A. Levenson, I. Abram, T. Rivera, P. Fayolle, J. C. Garreau, and P. Grangier, *Phys. Rev. Lett.* **70**, 267 (1993).
 - ¹¹ F. Helmer and F. Marquardt, *Phys. Rev. A* **79**, 052328 (2009).
 - ¹² L. S. Bishop, L. Tornberg, D. Price, E. Ginossar, A. Nunnenkamp, A. A. Houck, J. M. Gambetta, J. Koch, G. Johansson, S. M. Girvin, et al., *New Journal of Physics* **11**, 073040 (2009).
 - ¹³ A. Wallraff, D. I. Schuster, A. Blais, L. Frunzio, R. S. Huang, J. Majer, S. Kumar, S. M. Girvin, and R. J. Schoelkopf, *Nature (London)* **431**, 162 (2004).
 - ¹⁴ B. R. Johnson, M. D. Reed, A. A. Houck, D. I. Schuster, L. S. Bishop, E. Ginossar, J. M. Gambetta, L. DiCarlo, L. Frunzio, S. M. Girvin, et al., *Nature Physics* **6**, 663 (2010).
 - ¹⁵ N. Boulant, G. Ithier, P. Meeson, F. Nguyen, D. Vion, D. Esteve, I. Siddiqi, R. Vijay, C. Rigetti, F. Pierre, et al., *Phys. Rev. B* **76**, 014525 (2007).
 - ¹⁶ F. Mallet, F. R. Ong, A. Palacios-Laloy, F. Nguyen, P. Bertet, D. Vion, and D. Esteve, *Nature Physics* **5**, 791 (2009).
 - ¹⁷ T. Picot, A. Lupascu, S. Saito, C. J. P. M. Harmans, and J. E. Mooij, *Phys. Rev. B* **78**, 132508 (2008).
 - ¹⁸ T. P. Orlando, J. E. Mooij, L. Tian, C. H. van der Wal, L. S. Levitov, S. Lloyd, and J. J. Mazo, *Phys. Rev. B* **60**, 15398 (1999).
 - ¹⁹ J. E. Mooij, T. P. Orlando, L. Levitov, L. Tian, C. H. van der Wal, and S. Lloyd, *Science* **285**, 1036 (1999).
 - ²⁰ F. G. Paauw, A. Fedorov, C. J. P. M. Harmans, and J. E. Mooij, *Phys. Rev. Lett.* **102**, 090501 (2009).
 - ²¹ A. Fedorov, A. K. Feofanov, P. Macha, P. Forn-Diaz, C. J. P. M. Harmans, and J. E. Mooij, *Phys. Rev. Lett.* **105**, 060503 (2010).
 - ²² X. Zhu, A. Kemp, S. Saito, and K. Semba, *Appl. Phys. Lett.* **97**, 102503 (2010).
 - ²³ Y.-D. Wang, S. Chesi, D. Loss, and C. Bruder, *Phys. Rev. B* **81**, 104524 (2010).
 - ²⁴ I. Siddiqi, R. Vijay, F. Pierre, C. M. Wilson, M. Metcalfe, C. Rigetti, L. Frunzio, and M. H. Devoret, *Phys. Rev. Lett.* **93**, 207002 (2004).
 - ²⁵ A. Maassen van den Brink, A. J. Berkley, and M. Yalowsky, *New Journal of Physics* **7**, 230 (2005).
 - ²⁶ D. V. Averin and C. Bruder, *Phys. Rev. Lett.* **91**, 057003 (2003).
 - ²⁷ M. S. Allman, F. Altomare, J. D. Whittaker, K. Cicak, D. Li, A. Sirois, J. Strong, J. D. Teufel, and R. W. Simmonds, *Phys. Rev. Lett.* **104**, 177004 (2010).
 - ²⁸ Y. D. Wang, A. Kemp, and K. Semba, *Phys. Rev. B* **79**, 024502 (2009).
 - ²⁹ L. D. Landau and E. M. Lifshitz, *Mechanics* (Butterworth-Heinemann, 1976).
 - ³⁰ M. I. Dykman, *Phys. Rev. E* **75**, 011101 (2007).
 - ³¹ I. Serban, M. I. Dykman, and F. K. Wilhelm, *Phys. Rev. A* **81**, 022305 (2010).
 - ³² A. Lupascu, P. Bertet, E. F. C. Driessen, C. J. P. M. Harmans, and J. E. Mooij, *Phys. Rev. B* **80**, 172506 (2009).
 - ³³ A. Kemp, S. Saito, W. J. Munro, K. Nemoto, and K. Semba, arXiv:1008.4212 (2010).